Vinasse-based biochar magnetic composites: adsorptive removal of tetracycline in aqueous solutions

Yujia Xiang[1,2] · Yuzhou Zhou[2] · Bin Yao[2] · Yuqing Sun[3] · Eakalak Khan[4] · Wei Li[5] · Guihua Zeng[6] · Jian Yang[2] · Yaoyu Zhou[2]

Abstract

Highly efficient and cost-effective adsorbents for antibiotic removal are the key to mitigate pollution by industrial wastewaters. Pyrolyzing low-cost winemaking waste into biochar is a promising means for waste biomass utilization. This study assembled vinasse-derived biochar with manganese ferrite into vinasse-manganese ferrite biochar-magnetic composites (V-MFB-MCs) through simultaneous pyrolysis of waste biomass and metal (Mn and Fe) hydroxide precipitates. Batch experiments were conducted to evaluate the kinetics and isotherms of tetracycline (TC) adsorption as well as the influence of pH value, humic acid, and ionic strength. Morphological characterization showed that crystalline $MnFe_2O_4$ nanoparticles were impregnated within the framework of fabricated V-MFB-MCs. Superior TC adsorption capacity and fast pseudo-second-order kinetics could be achieved by the V-MFB-MCs-800 at pH 3.0. The TC adsorption onto V-MFB-MCs-800 was highly pH-dependent and controlled by the positive influence of ionic strength and humic acid. V-MFB-MCs-800 showed excellent adsorption performance in different natural water. Multiple interaction mechanisms including pore filling effect, π-π stacking interaction, and hydrogen bonding contribute to TC removal by V-MFB-MCs-800, which can be an innovative biowaste-derived material for industrial wastewater treatment.

Keywords Engineered biochar · Mineral biochar composites · Waste biomass valorization · Antibiotics removal · Wastewater treatment · Adsorption mechanism

Introduction

In the past few decades, the consumption of antibiotics that can prevent infections, treat diseases, and promote the growth of animals and humans has continuously increased worldwide (Alahabadi et al. 2017; Hosseini-Bandegharaei et al. 2016; Liu et al. 2018). However, antibiotics that can eliminate various species of microorganisms and stimulate evolution of "super-bacteria" could be directly released into the aquatic environment with potential ecological impacts (Gadipelly et al. 2014). Therefore, antibiotics have been

✉ Yuqing Sun
sun.yuqing@connect.polyu.hk

✉ Yaoyu Zhou
zhouyy@hunau.edu.cn

1 School of Environment and Energy, Guangdong Provincial Key Laboratory of Solid Wastes Pollution Control and Recycling, South China University of Technology, Guangzhou, Guangdong 510006, China

2 College of Resources and Environment, Hunan Agricultural University, Changsha 410128, China

3 Department of Civil and Environmental Engineering, The Hong Kong Polytechnic University, Hung Hom, Kowloon, Hong Kong, China

4 Department of Civil and Environmental Engineering and Construction, University of Nevada, Las Vegas, NV 89154, USA

5 School of Biology and Chemistry, Key Laboratory of Chemical Synthesis and Environmental Pollution Control-Remediation Technology of Guizhou Province, Xingyi Normal University for Nationalities, Xingyi 562400, China

6 Hunan Research Academy of Environmental Sciences, Changsha 410002, China

considered as nocuous, emerging environmental pollutants (Alahabadi et al. 2017). Particularly, tetracycline (TC), as an effective pharmaceutical ingredient, is extensively used in veterinary and aquaculture medicine for improving feed efficiencies and growth rates (Ji et al. 2011). Nevertheless, most of the TC used in the farming industry are excreted via feces and urine as un-metabolized matter, with only a handful of TC being metabolized (Zhao et al. 2012). Thus, agricultural fields receiving fertilizations of animal manures could be contaminated by TC that would consequently flow into different water bodies (e.g., rivers, lakes, and groundwater) due to surface runoff and infiltration and finally be accumulated in human bodies via intake of contaminated drinking water (Taheran et al. 2016; Xiang et al. 2022). Recently, the environmental incidents induced by TC pollution have attracted numerous attention worldwide and thus call for the imperative establishment of efficient, environmental-friendly treatment/remediation strategies (Xiong et al. 2018; Zhang et al. 2015).

Currently, TC can be removed from aquatic environments via different methods such as bioremediation (Singh et al. 2013), advanced oxidation processes (Sillanpää et al. 2011; Sun et al. 2019a; Zhou et al. 2018), and membrane processes (Xie et al. 2016). However, these traditional techniques have many limitations including high operational cost, non-centralized facilities, and complicated in situ management, which significantly inhibit their large-scale applications (Aghababaei et al. 2017). In contrast with the above methods, TC removal via the adsorption process is deemed as a more applicable, cost-effective, and sustainable practice (Yu et al. 2016; Zhou et al. 2019b, 2017).

Recently, biochars derived from cheap sources (e.g., agricultural wastes, forestry wastes, and industrial organic wastes) have been commonly selected as antibiotic adsorbents attributed to their wide applicability, high efficiency, and simple operation (Cui et al. 2016; Shakoor et al. 2019; Yao et al. 2013a; Zhou et al. 2019a). Biochars exhibit similar structures with activated carbon comprised of stacking graphite sheets but contain more diverse oxygen-carbon functional groups rimmed at the edges and forming connected microporous networks (Chen et al. 2007; Xiang et al. 2019a). Additionally, biochars also show potential applications for quality improvement (Shen et al. 2018; Silber et al. 2010; Xiang et al. 2020), contaminant immobilization (Wen et al. 2009), and carbon sequestration (Spokas and Reicosky 2009; Xiao et al. 2018) in soils. Due to their high specific surface area, porous structure, large pore volume (Ahmad et al. 2014; Lehmann et al. 2011), aromaticity, and high hydrophobicity (Ahmed et al. 2016; Lian et al. 2014), biochars are excellent adsorbents for antibiotics. However, adsorption affinity towards antibiotics was limited by the negatively charged surface of many biochars (Yao et al. 2013b), which can be mitigated by loading various metals

or metal oxides (e.g., Fe, Mn, and Al) via facile, one-step pyrolysis of biochar precursors pretreated with corresponding metal salts. Moreover, the impregnation of magnetic, nano-sized metals or metal oxides remarkably enhanced the performance and recoverability of biochars (Sun et al. 2019b; Tan et al. 2016; Xiang et al. 2019b).

In addition, ferrites with cubic spinel structures have attracted more attention owing to their relatively higher surface area, chemical stability under acidic conditions, and magnetic response than most of the metals or metal oxides (Jung et al. 2018). Specifically, manganese ferrite ($MnFe_2O_4$) nanoparticles wherein most of the trivalent cations (Fe^{3+}) and divalent ions (Mn^{2+}) predominantly occupy the octahedral and tetrahedral cationic sites (Reddy and Yun 2016), respectively, are of comparatively higher magnetic saturation and structural stability (Xiao et al. 2013; Xu et al. 2020). Thus, it could be speculated that integrating $MnFe_2O_4$ into a pristine biochar can further increase its TC adsorption capacity along with an easier separation of the spent adsorbents through an external magnetic field.

In this work, the innovative $MnFe_2O_4$/biochar magnetic composites were synthesized via co-precipitation of Mn and Fe onto vinasse-derived biochar, which were denoted as V-MFB-MCs (vinasse-manganese ferrite biochar-magnetic composites) here on, and tested for the TC removal from aqueous solutions. Vinasse that exhibits an awful odor, high organic content, low pH, good electric conductivity, and simple chemical compositions (Christofoletti et al. 2013; España-Gamboa et al. 2011) was recycled as biochar precursor due to its tremendous public concerns of indiscriminate disposal and insufficient management (Christofoletti et al. 2013), which has incurred serious adverse impacts on human and animal life, agricultural soils, rivers, and lakes (Christofoletti et al. 2013). The acquired V-MFB-MCs were comprehensively characterized for their physicochemical properties, crystalline structure, and surface chemical behavior. The experimental influencing factors (e.g., solution pH, TC concentrations, ionic strength, humic acid, and reaction time) were systematically investigated. The TC adsorption mechanisms were illustrated in detail in accordance with the studies of adsorption isotherms and kinetics. These results of the study should be beneficial to promote the future design of high-performance, sustainable, and engineered biochar composites for environmental applications.

Materials and methods

Biomass and chemicals

Vinasse (LIQUOR CO., LTD., Jishou, Hunan, China) was selected as feedstock to produce biochar. TC was obtained from Macklin (Shanghai, China). All chemical reagents used

in this study were purchased from Sigma-Aldrich (USA) and of analytical grade without further purification. The deionized (DI) water (18.2 MΩ·cm) was used in the experiments.

Synthesis of V-MFB-MCs

The V-MFB-MCs were synthesized via a co-precipitation method reported in previous studies (Jung et al. 2017, 2018). The as-received vinasse was completely air-dried and then ground to pass a 20-mesh sieve (< 0.9 mm). A mass of 5.0 g vinasse was transferred into 100 mL DI water and homogeneously mixed for 30 min at 200 rpm. Then, certain amounts of $FeCl_3 \cdot 6H_2O$ (10.8120 g, 0.04 mol) and $MnCl_2 \cdot 4H_2O$ (3.9582 g, 0.02 mol) were added into this mixture. Next, the solution pH was adjusted to 10.0 by adding NaOH (5 M) drop-wise followed by 4 h oven-dry (60 °C) with continuously mixing. The obtained solid was filtered, repeatedly washed by DI water, and subsequently oven-dried at 100 °C for 24 h. The solid was further pyrolyzed in a quartz tubular furnace (OTF-1200X, Hefei Kejing Materials Technology Co., LTD., China) at different pyrolysis temperatures (i.e., 400, 600, and 800 °C) with the heating rate of 7 °C/min for 1 h under N_2 atmosphere (N_2 purging rate of 100 mL min^{-1}), which were labeled as V-MFB-MCs-400, V-MFB-MCs-600, and V-MFB-MCs-800, respectively. After cooling down to room temperature with continuous N_2 purging, the product was carefully washed by DI water until reaching neutral pH. Finally, the sample was oven-dried at 100 °C for 24 h and ground to pass a 100-mesh sieve (< 0.15 mm). The pristine biochar (PBC) was obtained via the vinasse pyrolyzed in a quartz tubular furnace under the same condition, which was labeled as PBC-400, PBC-600 and PBC-800, respectively. The acquired V-MFB-MCs and BC were stored in a sealed container before use.

Microscopic characterization of V-MFB-MCs

The specific surface areas and porosity of V-MFB-MCs and PBC were determined by the Brunauer–Emmett–Teller (BET) method and Barret–Joyner–Halenda (BJH) method with Micromeritics ASAP 2020 based on adsorption isotherms of nonreactive $N_2(g)$. XRD test was conducted to determine the phase compositions of the samples on a Bruker X-ray diffractometer (XRD, D8 Advance, Bruker, Germany) with Cu-Kα radiation (λ = 1.5418 Å) in continuous scanning mode and performed at 40 kV and 40 mA. Fourier transform infrared (FT-IR) spectra were recorded using a FT-IR spectrometer in the 4000–650 cm^{-1} range (Spectrum 3, PerkinElmer, USA). The characteristics of the V-MFB-MCs-800 were identified via scanning electron microscope (SEM, Quanta FEG 450, FEI, USA), transmission electron microscopy (TEM, HT7700, Hitachi, Japan), and X-ray photoelectron spectroscopy (XPS, Escalab 250Xi, Thermo Fisher

Scientific, USA). Zeta potential of the V-MFB-MCs was determined by a Nano Zetasizer (Omni, Brookhaven, USA).

Removal of TC by V-MFB-MCs

Removal of TC by the V-MFB-MCs under different influencing factors, such as solution pH (3, 4, 5, 6, 7, 8, 9, 10, and 11), initial TC concentration (5–700 mg/L), humic acid (0–50 mg/L), ionic strength (NaCl, $NaNO_3$, Na_2SO_4), and contact time (5–4320 min), was systematically investigated. The experiments were conducted in 100-mL polyethylene plastic bottles under continuously agitation (200 rpm) in a water bath shaker (SHA-C, Changzhou Aohua Instrument Co., Ltd., China). The solution pH was adjusted with HCl (0.1 M) or NaOH (0.1 M). After reaction, the samples were filtered by a disposable 0.45-μm polyvinylidene fluoride (PVDF) filter (Millipore, USA), and the supernatant was analyzed for TC concentration. To estimate the adsorption performance of V-MFB-MCs in diverse water bodies (such as DI water, bottled water, tap water, lake water obtained from South China University of Technology Lake located in Guangzhou, and Zhujiang water obtained from the Pearl River) were used to study, which were directly employed to prepare TC solution without filtration.

Analytical methods

The adsorption kinetics of TC was described by the following kinetic models (Tang et al. 2018):

$$\text{Pseudo} - \text{first} - \text{order} : q_t = q_e(1 - \exp(-k_1 t)) \tag{1}$$

$$\text{Pseudo} - \text{second} - \text{order} : q_t = \frac{q_e^2 k_2 t}{1 + q_e k_2 t} \tag{2}$$

$$\text{Evolich} : q_t = \alpha + k_e lnt \tag{3}$$

$$\text{Bangham} : lgq_t = \frac{1}{m}lgt + lgk \tag{4}$$

$$\text{Intra} - \text{particle diffusion} : q_t = k_i t^{1/2} + c_i \tag{5}$$

where q_e and q_t are the adsorption capacities (mg/g) of adsorbent towards TC at equilibrium and time t (min), respectively; k_1 (1/min), k_2 (g/mg·min), k_i (mg/g·min$^{0.5}$), k_e, k, and m are the respective rate constants; c_i is the intercept related to the thickness of the boundary layer.

Different adsorption isotherms (Langmuir, Freundlich, and Temkin models) were adopted to fit the data of adsorption isotherm experiments (Tang et al. 2018):

Langmuir : $q_e = \dfrac{K_L q_m C_e}{1 + C_e}$ (6)

Freundlich : $q_t = K_F t^{-n}$ (7)

where C_e is the TC concentration at equilibrium (mg/L); q_m is the maximum adsorption capacity (mg/g); K_L (L/mg) and K_F (L/mg) are the respective adsorption constants; and n indicates the adsorption intensity.

The solution pH was monitored using a pH meter (PHS-3C, Shanghai INESA Scientific Instrument Co., Ltd, China). TC concentration was determined by a UV–Vis spectrophotometer (UV2600, Shimadzu, limit of detection of 0.24 mg/L) (Fernández-Calviño et al. 2015). All experiments were performed in triplicate, and the results are presented as mean ± standard deviations.

Results and discussion

Effects of modification and pyrolysis temperatures

As modification and pyrolysis temperatures generally showed a huge effect on the biochar properties, modification (vinasse biochars without modification and with modified by ferrites) and three pyrolysis temperatures (400, 600, and 800 °C) of biochars were taken into account. Visually different from the PBC, V-MFB-MCs were more fine and exquisite grains. Moreover, the adsorbents pyrolyzed at 600 and 800 °C showed a completely black color, while the adsorbents pyrolyzed at 400 °C presented the yellow–brown, which was due to imperfect carbonization (Tang et al. 2018).

Based on nitrogen adsorption–desorption analysis, both modification and pyrolysis temperatures could greatly change the biochars' porosity. As shown in Table 1, the BET surface area of V-MFB-MCs-800 (161.174 m^2/g) was much higher than that of PBC-800 with the total pore volume raising to 0.191 cm^3/g, which might result in its strong TC adsorption. Meanwhile, higher pyrolysis temperature could promote the breakage of weak bonds along with more loss

of H, N, and O, which might be an important reason for the increase in pore volume and BET. There was no doubt about the increased pore volume and BET could improve the adsorption ability of materials.

According to the XRD patterns in the range of 5–80° presented in Fig. S1a, it was shown that pyrolysis temperature was crucial to the formation of ferrites with cubic spinel structures. The reflection peaks of the V-MFB-MCs were found at 2θ of 35.44°, 41.16°, 59.62°, 71.31°, and 75.00° with d-spacing values of 2.531, 2.192, 1.550, 1.322, 1.265, and 1.096 Å, respectively. The observed peaks represented crystallographic planes (khl) (1 1 1), (2 0 0), (2 2 0), (3 1 1), (2 2 2), and (4 0 0), respectively, which were in accordance with the cubic spinel structure (JCPDS No. 01–077-2359). Only when the firing temperature reaches 800 °C will the ferrites with cubic spinel structures be formed. Furthermore, higher pyrolysis temperature could increase the degree of graphitization.

The FTIR spectra was conducive to verify the functional groups on the V-MFB-MCs and PBC surface (Fig. S1b). The small bands at 1600 cm^{-1} and 15,860 cm^{-1} were consistent with the stretching vibration of C=O in carboxylic group (Xiong et al. 2018), whereas the spectral band with a peak at 1367 cm^{-1}, 962 cm^{-1}, and 900 cm^{-1} was ascribed to the presence of the –OH group (Daifullah and Girgis 2003, Pezoti et al. 2016). The spectral band with a peak at 1118 cm^{-1} was attributed to C–O surface functional group (Pezoti et al. 2016). Based on the FTIR result, the modification brought more oxygen-containing functional groups to the materials. As the pyrolysis temperature increased, the intensity of bands at 795 cm^{-1} decreased, suggesting the relative number of substituents on the aromatic ring decreased. It was mainly due to the aromatization degree and unsaturated bonds of materials increased, and the polarity of materials decreased along with the pyrolysis temperature increased.

Thermal stabilities of the V-MFB-MCs and PBC were studied by TG analysis ranging from 30 to 800 °C with a heating rate of 10 °C /min under nitrogen atmosphere (Fig. S1c). TG analysis results showed that pyrolysis temperature had a greater effect on the stabilities of materials than modification. In the range from 30 to 200 °C, there was a weight loss, which mainly was attributed to

Table 1 Porosity characteristic of vinasse biochars

Classifications	Materials	BJH pore diameter (nm)	BET surface area (m^2/g)	Total pore volume (cm^3/g)	Qe for TC (C_0 = 100 mg/L)
Vinasse biochars without modification (PBC)	PBC-400	154.988	2.284	0.00885	56.41
	PBC-600	131.414	2.884	0.00948	68.20
	PBC-800	173.860	2.859	0.0124	78.74
Vinasse biochars modified by ferrites (V-MFB-MCs)	V-MFB-MCs-400	61.833	103.927	0.161	108.75
	V-MFB-MCs-600	48.093	112.170	0.135	110.59
	V-MFB-MCs-800	47.281	161.174	0.191	331.50

the removal of pre-adsorptive water molecules on the samples (Pezoti et al. 2016). Subsequently, the second mass loss of materials at medium–high temperature range (200 − 600 °C) can be due to the main component decomposition of waste biomass (cellulose, lignin, and hemicellulose) (Yang et al. 2019), whereas the weight of V-MFB-MCs-800 kept little changed with the increase of the temperature (range from 200 to 700 °C), showing its high thermal stability in the temperature range from 30 to 800 °C. Because V-MFB-MCs-800 had a higher specific surface area, better stability, and more excellent adsorption performance, the next work would focus on V-MFB-MCs-800.

Physiochemical properties and surface chemical behavior of V-MFB-MCs-800

Figure 1 provided the SEM and TEM images of the V-MFB-MC-800. As shown in Fig. 1a, V-MFB-MCs-800 had a cylindrical shape with a lot of pores on its surface, which

is conducive to TC adsorption. A great deal of agglomerated particles with diameter ranges from micro to nanoscale was observed on the irregular surface of V-MFB-MCs-800, speculating the possible formation of Mn and Fe oxides. Additionally, the TEM images of the V-MFB-MCs-800 (Fig. 1b) gave evidences that nanoscale mineral rods in the range of 40–100 nm were formed.

The XPS survey showed that the V-MFB-MCs were composed of Fe 2p, Mn 2p, O 1 s, and C 1 s (Fig. 2a). The O 1 s spectra (Fig. S1d) were composed of one predominant peak that was assigned to the lattice of O atoms that were combined with Fe and Mn at around 530 eV (Wang et al. 2017). In addition, as illustrated in Fig. 2b, Fe 2p spectrum showed two typical peaks located at 725.0 and 711.3 eV, which were consistent with Fe $2p_{1/2}$ and Fe $2p_{3/2}$ of Fe^{3+} cations, respectively. Furthermore, the Mn 2p spectrum (Fig. 2c) revealed two representative peaks at binding energy of 653.5 and 641.8 eV, which were correlated with the typical doublets of Mn $2p_{1/2}$ and Mn $2p_{3/2}$, respectively, manifesting the oxidation state of Mn^{2+} in $MnFe_2O_4$ (Long et al. 2017; Zhang

Fig. 1 **a** SEM and **b** TEM images of the V-MFB-MCs-800 (SEM scale bar: 100 μm; TEM scale bar: 200 nm)
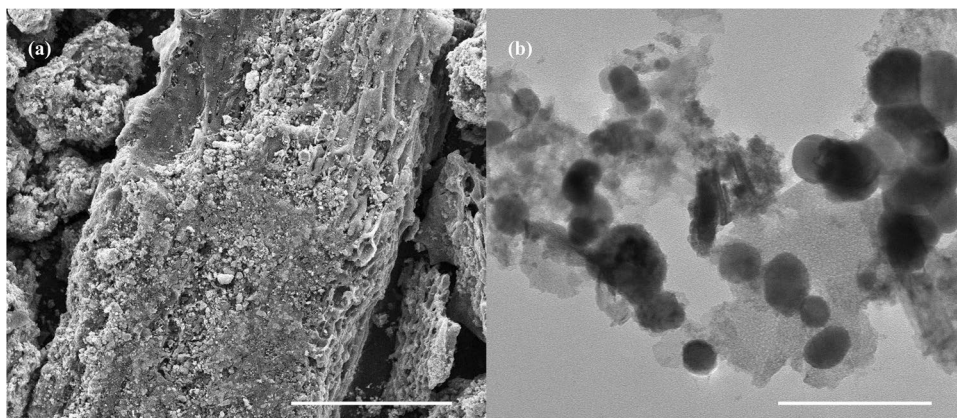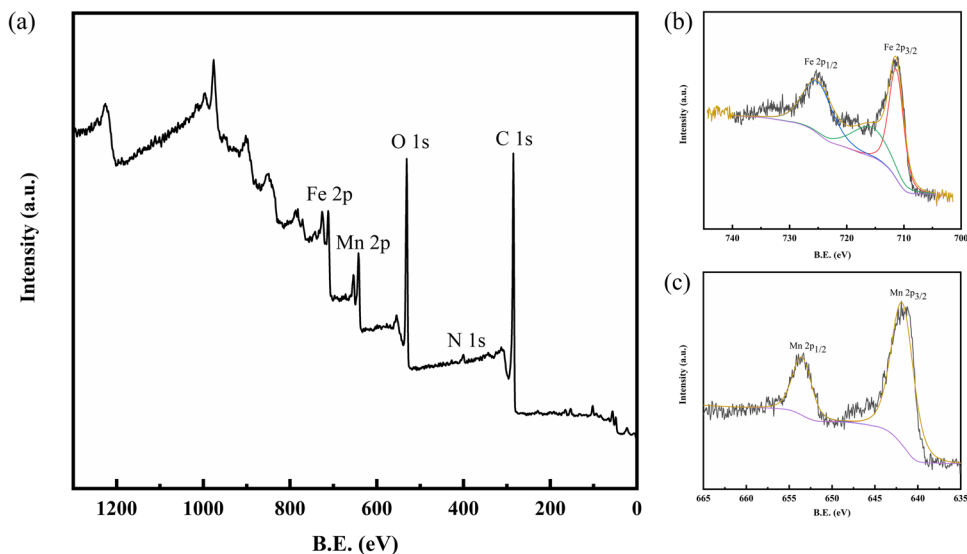

Fig. 2 **a** XPS full-survey and XPS analysis of **b** Fe 2p, **c** Mn 2p binding states of the V-MFB-MCs-800

et al. 2013). These results corresponded to the XRD findings concerning the Fe^{3+}, Mn^{2+}, Fe–O, and Mn–O species in V-MFB-MCs. It was previously reported that the Fe^{3+} ions firstly formed $Fe(OH)_3$ by the hydrolysis process. Subsequently, $Fe(OH)_3$ was reduced by strong alkali to $MnFe_2O_4$ monomers and/or Fe_3O_4 monomers that corresponded to the XRD (Long et al. 2017).

V-MFB-MCs for TC removal

Kinetics

The TC adsorption by the V-MFB-MCs-800 as a function of time (Fig. 3a) manifested that the TC adsorption capacity raised with reaction time until adsorption sites of adsorbent were progressively taken up and achieved apparent adsorption equilibrium. In terms of multilinearity of TC adsorption showed in Fig. 3a and d and Table S1, the sharp and fast initial region (0–480 min) was attained, which is attributed to the abundance of TC and binding sites in aqueous solution. In this case, the adsorption of TC carried on through either external surface adsorption (film diffusion) or rapid boundary layer diffusion on the external surface (instantaneous adsorption). Afterwards, the second region (480–2160 min) described the diffusion of TC molecules into porous structure of V-MFB-MCs-800. Eventually, the last region

(2160–4320 min) portrayed the achievement of adsorption equilibrium, when the intraparticle diffusion started to slow down because of the low TC levels in the water solution.

The fitting parameters attained from pseudo-first-order, pseudo-second-order, Elovich model, and Bangham kinetic models were summarized in Table 2 and Fig. 4. The TC adsorption data for V-MFB-MCs-800 were best fitted by pseudo-second-order kinetic model with the relatively high coefficients of correlation ($R^2 = 0.993$), which may infer the chemical adsorption as the rate-limiting step (Tang et al. 2017, 2018). The TC adsorption behaviors onto V-MFB-MCs-800 were further studied by Elovich and Bangham models. Elovich model ($R^2 = 0.969$) manifested wide-ranging control of heterogeneous diffusion factors, where the rate constant ($k_e = 58.27$) showed TC adsorption speed onto the V-MFB-MCs-800. Meanwhile, Bangham model showed comparatively good linearity ($R^2 = 0.959$), reflecting the channel diffusion process existence in TC adsorption process of V-MFB-MCs-800.

Adsorption isotherms

The equilibrium adsorption isotherms of V-MFB-MCs-800 after 24-h reaction at different temperatures were depicted in Fig. S2, showing the TC adsorption capacity

Fig. 3 Kinetics of TC adsorption onto V-MFB-MCs-800 by fitting the **a** pseudo-first-order, **a** pseudo-second-order model, **b** Elovich model, **c** Bangham fitting model, **d** intra-particle diffusion model
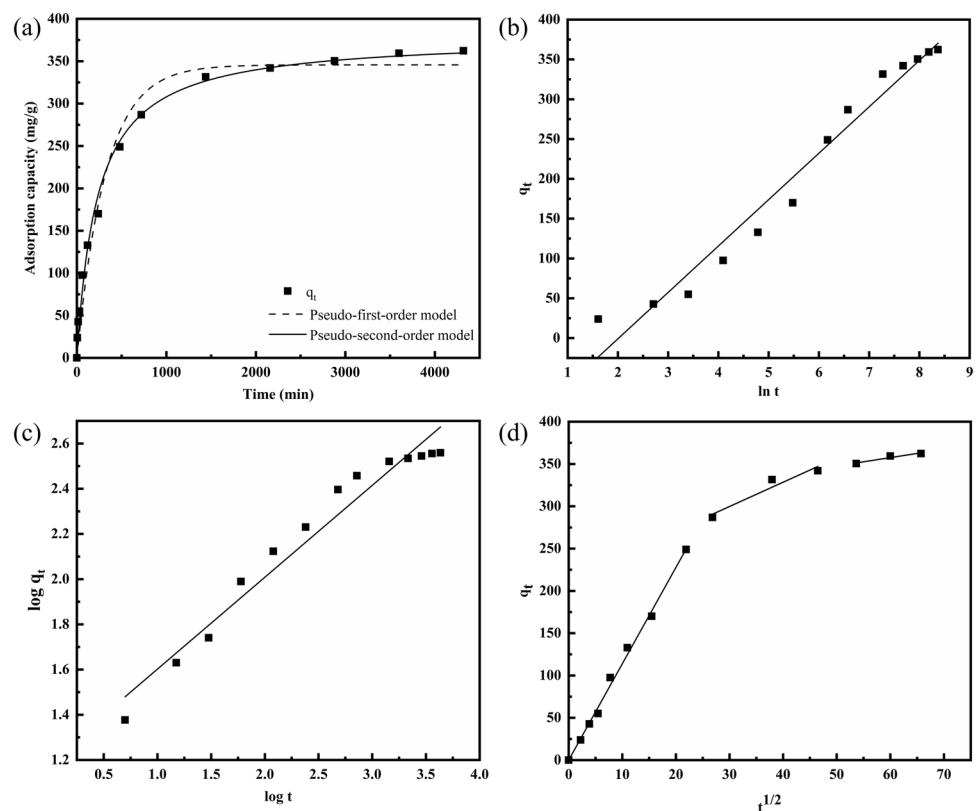
Table 2 Kinetic parameters for TC adsorption onto the V-MFB-MCs-800

Kinetics models	Parameters	
Experimental results	q_{exp}	362.22
Pseudo-first-order	q_e	345.67
	k_1	3.10×10^{-3}
	R^2	0.978
Pseudo-second-order	q_e	379.06
	k_2	1.14×10^{-5}
	R^2	0.993
Elovich model	k_e	58.27
	α	-117.45
	R^2	0.969
Bangham model	k_b	15.68
	m	2.46
	R^2	0.959

onto V-MFB-MCs-800 increased with the increase of the initial TC concentration and reaction temperature. The Langmuir and Freundlich models (results presented in Table S2) portrayed the isotherm data pretty well, of which R^2 values were not much different. As for Langmuir model, the rising reaction temperature brought with the q$_m$ and K$_L$ values increased along with the reaction temperature raised, indicating that the higher temperature could upgrade the adsorption process through reinforcing the bonding between the TC and active sites of V-MFB-MCs-800 (Tang et al. 2018). The highly linear relationship of Freundlich model could reveal that physical interaction has a vital effect on the adsorption process that of Langmuir model could manifest that adsorption process closely relate to chemical adsorption. According to the high linear fitting of two representative models, it can infer that both physical and chemical interactions were crucial for TC adsorption process onto V-MFB-MCs-800. The V-MFB-MCs-800 indicated significant adsorption affinity towards TC with maximum TC adsorption of 331 mg/g at 25 °C. It was worth noticing that the adsorption capacity of V-MFB-MCs-800 in the study was visibly higher than other previously reported adsorbents (Table 3). These comparisons manifested the potential of V-MFB-MCs-800 as a promising and effective adsorbent.

Effects of pH values and ionic strengths on TC removal

Figure 4a depicted the effect of solution initial pH values on the TC adsorption onto V-MFB-MCs-800. It can be seen that adsorption of TC on V-MFB-MCs-800 was highly pH dependent and the adsorption capacity steadily decelerated with the increase of pH ranging from 3.0 to 11.0. Figure 4a depicted the highest TC adsorption

capacity of V-MFB-MCs-800 as 323 mg g^{-1} at a pH value of 3.0. Thus, the corresponding pH value of 3.0 was accordingly considered as the optimal pH value for TC adsorption onto the V-MFB-MCs-800.

The obvious difference of TC removal by the V-MFB-MCs-800 at varied pH values of the solution was most likely attributed to the TC speciation, composite surface charge, and subsequent interaction between them. As shown in Fig. 4a, zeta potential presented a pronounced decreasing trend as pH increased. The speciation of TC, as an amphoteric molecule, could be developed with various pH values due to fluctuation in the protonation-deprotonation reactions of three different groups in TC. At a lower pH value (i.e., $pH = 3.0$), TC was completely protonated and exhibited one positive charge (H$^+$). Hence, in addition to the π-π interaction between aromatic ring structure of TC (electron donor) and graphite-like structure of BC (π-acceptor) (Liu et al. 2012; Taheran et al. 2016), H-π bonding could also be stimulated for increased adsorption of an ionized compound by BC (Jung et al. 2013). However, at slightly higher pH, deprotonation of the first group in TC ($pKa = 3.3$) took place, which led to the formation of a neutral-charged species. Then, deprotonation of the second group in TC kicked in with $pKa = 7.7$ to generate a species that presented one negative charge (Taheran et al. 2016). Next, with continuously increased solution pH, the third group in TC deprotonated ($pKa = 9.7$), producing a species with two negative charges (Parolo et al. 2008). Therefore, the more alkaline environment at higher pH (i.e., $pH = 5.0–11.0$) adversely influenced TC uptake by the adsorbent because of the intensified electrostatic repulsion and inhibited H-π bonding.

Humic acid (HA) is widely present in aqueous solutions obtained by microorganisms degrading dead plants and other substances. Thus, this study investigated the effects of different doses HA on TC adsorption. As seen in Fig. 4b, with the increase of HA concentration, the adsorption capacity of TC also increased, indicating HA can promote TC adsorption. This may be because V-MFB-MCs-800 adsorb HA via hydrogen bonding or electrostatic interaction, and HA can act as a "bridging" on the surface of V-MFB-MCs-800 to form new adsorption sites (Lian et al. 2015).

Inorganic anions frequently coexist with TC in industrial wastewater, which probably interrupts the TC adsorption process. Therefore, the influence of ionic strength on the adsorption process of TC was conducted here by the addition of different doses NaCl, NaNO$_3$, and Na$_2$SO$_4$ (from 0 to 0.05 mol/L) to the solution. As shown in Fig. 4c, increasing ionic strength (NaCl, NaNO$_3$, and Na$_2$SO$_4$ concentration) from 0 to 0.05 mol/L gradually promoted TC adsorption onto V-MFB-MCs-800,

Fig. 4 Effects of **a** pH, **b** humic acid, and **c** inorganic salt on TC adsorption process (TC concentration: 100 mg/L, adsorbent dose = 0.1 g/L, T = 25 °C). Bar charts and circles represented adsorption capacity and zeta potential of the V-MFB-MCs-800, respectively. **d** TC adsorption by V-MFB-MCs-800 in different water samples (TC concentration: 100 mg/L, adsorbent dose = 0.1 g/L, T = 25 °C)
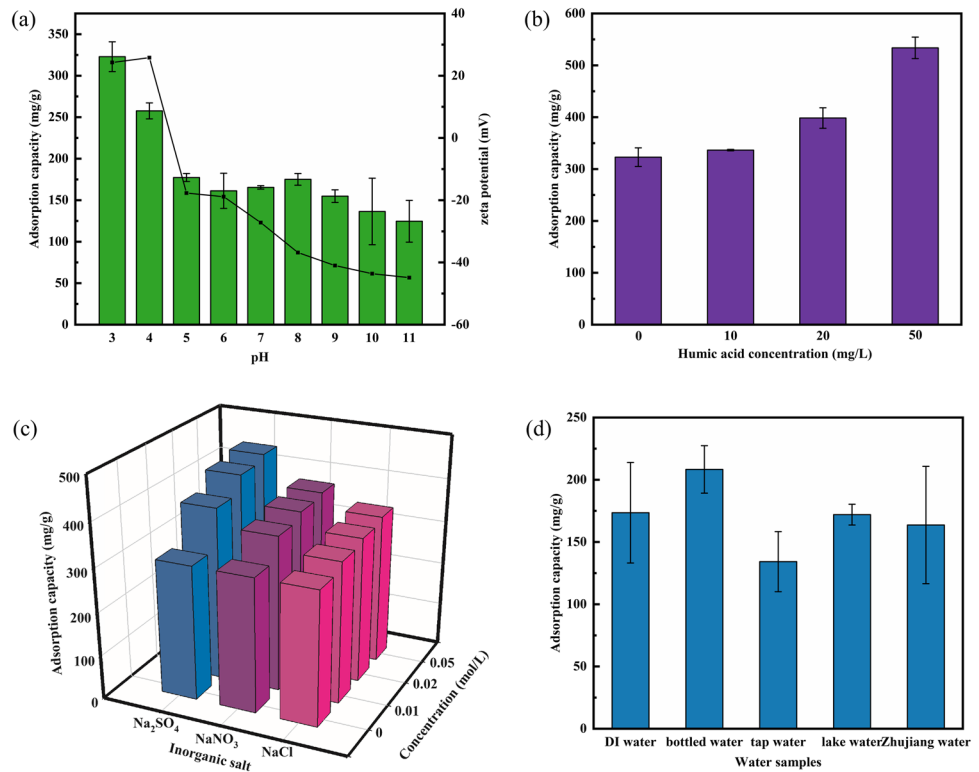
suggesting V-MFB-MCs-800 was suitable for eliminating TC in industrial wastewater. Thus, the higher salt concentration may impose a "salting-out effect" and non-electrostatic forces on TC, thereby enhancing the partitioning/penetration of the compound into the adsorbent (Lei et al. 2018; Peng et al. 2018).

Application on natural water

The study of TC adsorption properties on V-MFB-MCs-800 in DI water, bottled water, tap water, lake water, and Zhujiang, water was shown in Fig. 4d. Obviously, the adsorption of TC in tap water was significantly inhibited, which may be

Table 3 Comparison of tetracycline antibiotics adsorption capacity of various adsorbents

Antibiotics	Adsorbent	C_0 (mg/L)	T (°C)	pH	BET surface area (m²/g)	Total pore volume (cm³/g)	Adsorption capacity Q (mg/g)	Reference
Tetracycline	V-MFB-MCs-800	100	25	3.0	161.174	0.191	331	This study
Tetracycline	Ori-char	100	30	2.0	51.9	0.031	81.0	(Jing et al. 2014)
Tetracycline	MeOH-char	100	30	2.0	66.0	0.051	95.6	(Jing et al. 2014)
Tetracycline	Alkali biochar	–	30	Unadjusted	118	0.073	58.8	(Liu et al. 2012)
Tetracycline	Acid biochar	–	30	Unadjusted	46.8	0.033	23.3	(Liu et al. 2012)
Tetracycline	Bamboo charcoal	–	30	7.0	67.8	0.024	22.7	(Liao et al. 2013)
Tetracycline	GO-MPs	–	–	–	–	–	39.1	(Lin et al. 2013)
Chlortetracycline	GO-MPs	–	–	–	–	–	42.6	(Lin et al. 2013)
Oxytetracycline	GO-MPs	–	–	–	–	–	45.0	(Lin et al. 2013)
Doxycycline	GO-MPs	–	–	–	–	–	35.5	(Lin et al. 2013)
Chlortetracycline hydrochloride	MWCNT	–	25	7.0	137	0.400	39.3	(Xiong et al. 2018)
Oxytetracycline	MWCNT	–	23	7.0	86.0	0.319	73.0	(Oleszczuk and Xing 2011)
Oxytetracycline hydrochloride	MWCNT	–	25	7.0	137	0.400	54.1	(Xiong et al. 2018)

related to the pH of the tap water. In particular, the adsorption capacity of TC in DI water was not much different from lake water and Zhujiang water, suggesting V-MFB-MCs-800 can be expected to be applied to natural water bodies.

TC adsorption mechanism

It is well-known that both physisorption and chemisorption significantly contributed to the high adsorption capacity of TC. Generally speaking, physical adsorption primarily corresponded to pore structures properties of adsorbents, and chemical adsorption mainly correlates with functional groups onto the surface of adsorbents. In this work, after the modification of PBC, the BET surface area, pore diameters, and total pore volume highly increased, resulting in a significant increase of TC adsorption capacity. Hence, it was suggested that pore filling effect contributed to the efficient adsorption of TC.

To gain investigation into the TC adsorption mechanisms onto V-MFB-MCs-800, FTIR and XPS studies before and after adsorption were carried out. The FTIR spectra of V-MFB-MCs-800 (Fig. S3) revealed the decreased intensity and shifted peak position approximated at 920 cm^{-1} after TC loading on the composites; hence, the TC removal might be due to the interaction with hydrogen bonding [61] and π-hydrogen bonding [62]. Comparing the C 1 s survey of V-MFB-MCs-800 before and after TC adsorption, the peak ratio assigned to C–C/C = C notably increased (Fig. S4), indicating that TC was removed via π-π interaction (Tian et al. 2017). When at $pH = 3.0$, both V-MFB-MCs

and TC were positively charged; hence, there was a little electrostatic attraction between V-MFB-MCs-800 and TC. Herein, it was previously reported that feeble electrostatic attraction could narrow molecule distances between adsorbents and adsorbates, thereby facilitating the formation of π-π stacking interaction between adsorbents and adsorbates (Tian et al. 2017). Thus, π-π stacking interaction was seen as the prominent chemical driving force in this study. Meanwhile, cation-π interaction would also exist between TC with V-MFB-MCs-800 because of the strong electron donor ability of V-MFB-MCs-800 and high acceptance ability electronic of TC (Tang et al. 2018).

In order to investigate electrostatic interaction in the adsorption process, the correlation between pH values and TC adsorption capability was studied. The highest adsorption capacity of TC occurred at the pH of 3.0; subsequently, the TC adsorption capacity decreased with solution pH increase. Therefore, the electrostatic attraction was not the prominent mechanism in the adsorption process. Integrated the above analysis, the TC adsorption mechanisms on V-MFB-MCs-800 probably consisted of pore filling, hydrogen bonding, cation-π interaction, and π-π stacking interaction, which can be vividly illustrated in Fig. 5.

Conclusion

The V-MFB-MCs-800 can be synthesized by a trouble-free co-precipitation method followed by high-temperature pyrolysis, showing the promising TC adsorption capacity.

Fig. 5 Schematic diagram of possible mechanisms of TC adsorption onto the V-MFB-MCs-800
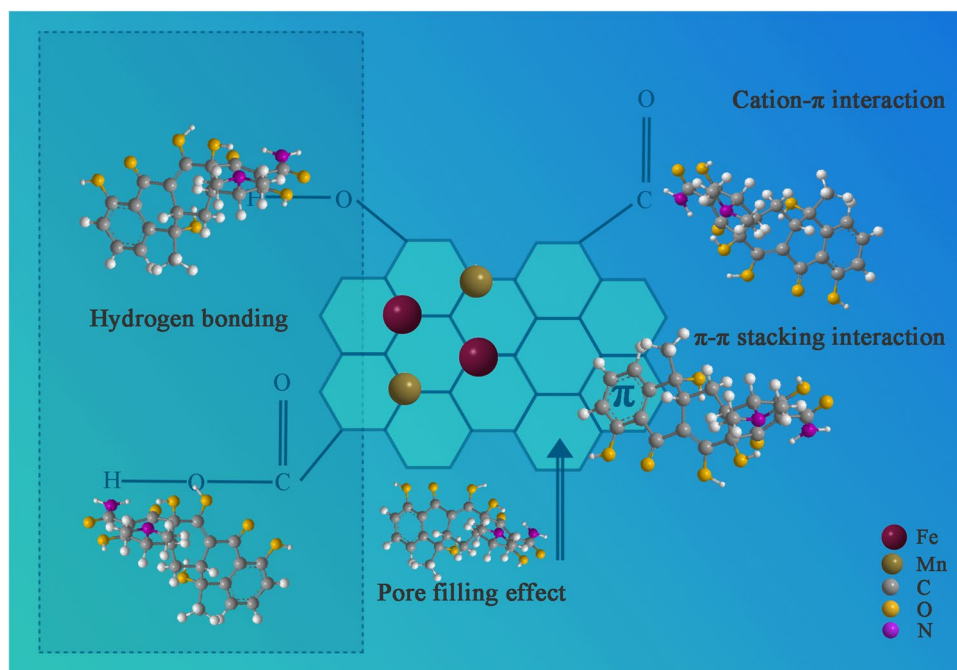
The resulting V-MFB-MCs-800 was characterized by SEM, TEM, XRD, XPS, and FTIR, which could confirm the homogeneous impregnation of Fe_3O_4 and/or $MnFe_2O_4$ nanoparticles on the surface of BC with hierarchical pores. Multiple interaction mechanisms involved the pore filling effect, hydrogen bonding (–OH vibration peaks changed), π-π stacking interaction (C–C/C = C bond area changed), and cation-π interaction (–C = O peak changed). The co-existence of inorganic anions exerted a positive influence on the removal capacity via "salting-out" effect and non-electrostatic forces. Ionic strengths/HA/natural water tests further suggested that V-MFB-MCs-800 can be potentially applied for TC removal from wastewater.

Author contribution YX: conceptualization, investigation, writing—original draft, writing—original revise.

YZ: investigation, supervision, writing—review and editing.

BY: investigation, supervision, writing—review and editing.

YS: conceptualization, supervision, project administration, writing—review and editing.

EK: supervision, writing—review and editing.

WL: supervision, writing—review and editing.

GZ: supervision, writing—review and editing.

JY: supervision, writing—review and editing.

YZ: conceptualization, supervision, project administration, funding acquisition, writing—review and editing.

Data availability The experimental data and materials during the current study are available from the first author on reasonable request.

Declarations

Ethics approval and consent to participate Not applicable.

Consent for publication Not applicable.

Competing interests The authors declare no competing interests.

References

Aghababaei A, Ncibi MC, Sillanpää M (2017) Optimized removal of oxytetracycline and cadmium from contaminated waters using chemically-activated and pyrolyzed biochars from forest and wood-processing residues. Biores Technol 239:28–36

Ahmad M, Rajapaksha AU, Lim JE, Zhang M, Bolan N, Mohan D, Vithanage M, Lee SS, Ok YS (2014) Biochar as a sorbent for contaminant management in soil and water: a review. Chemosphere 99:19–33

Ahmed MB, Zhou JL, Ngo HH, Guo W (2016) Insight into biochar properties and its cost analysis. Biomass Bioenerg 84:76–86

Alahabadi A, Hosseini-Bandegharaei A, Moussavi G, Amin B, Rastegar A, Karimi-Sani H, Fattahi M, Miri M (2017) Comparing adsorption properties of NH4Cl-modified activated carbon towards chlortetracycline antibiotic with those of commercial activated carbon. J Mol Liq 232:367–381

Chen W, Parette R, Zou J, Cannon FS, Dempsey BA (2007) Arsenic removal by iron-modified activated carbon. Water Res 41:1851–1858

Christofoletti CA, Escher JP, Correia JE, Marinho JFU, Fontanetti CS (2013) Sugarcane vinasse: environmental implications of its use. Waste Manage 33:2752–2761

Cui E, Wu Y, Zuo Y, Chen H (2016) Effect of different biochars on antibiotic resistance genes and bacterial community during chicken manure composting. Biores Technol 203:11–17

Daifullah A, Girgis B (2003) Impact of surface characteristics of activated carbon on adsorption of BTEX. Colloids Surf A Physicochem Eng Asp 214:181–193

España-Gamboa E, Mijangos-Cortes J, Barahona-Perez L, Dominguez-Maldonado J, Hernández-Zarate G, Alzate-Gaviria L (2011) Vinasses: characterization and treatments. Waste Manag Res 29:1235–1250

Fernández-Calviño D, Bermúdez-Couso A, Arias-Estévez M, Nóvoa-Muñoz JC, Fernández-Sanjurjo MJ, Álvarez-Rodríguez E, Núñez-Delgado A (2015) Competitive adsorption/desorption of tetracycline, oxytetracycline and chlortetracycline on two acid soils: stirred flow chamber experiments. Chemosphere 134:361–366

Gadipelly C, Pérez-González A, Yadav GD, Ortiz I, Ibáñez R, Rathod VK, Marathe KV (2014) Pharmaceutical industry wastewater: review of the technologies for water treatment and reuse. Ind Eng Chem Res 53:11571–11592

Hosseini-Bandegharaei A, Alahabadi A, Rahmani-Sani A, Rastegar A, Khamirchi R, Mehrpouyan M, Agah J, Pajohankia Z (2016) Effect of nitrate and amine functionalization on the adsorption properties of a macroporous resin towards tetracycline antibiotic. J Taiwan Inst Chem Eng 66:143–153

Ji L, Wan Y, Zheng S, Zhu D (2011) Adsorption of tetracycline and sulfamethoxazole on crop residue-derived ashes: implication for the relative importance of black carbon to soil sorption. Environ Sci Technol 45:5580–5586

Jing X-R, Wang Y-Y, Liu W-J, Wang Y-K, Jiang H (2014) Enhanced adsorption performance of tetracycline in aqueous solutions by methanol-modified biochar. Chem Eng J 248:168–174

Jung C, Park J, Lim KH, Park S, Heo J, Her N, Oh J, Yun S, Yoon Y (2013) Adsorption of selected endocrine disrupting compounds and pharmaceuticals on activated biochars. J Hazard Mater 263:702–710

Jung K-W, Lee S, Lee YJ (2017) Synthesis of novel magnesium ferrite (MgFe2O4)/biochar magnetic composites and its adsorption behavior for phosphate in aqueous solutions. Biores Technol 245:751–759

Jung K-W, Lee SY, Lee YJ (2018) Facile one-pot hydrothermal synthesis of cubic spinel-type manganese ferrite/biochar composites for environmental remediation of heavy metals from aqueous solutions. Biores Technol 261:1–9

Lehmann J, Rillig MC, Thies J, Masiello CA, Hockaday WC, Crowley D (2011) Biochar effects on soil biota–a review. Soil Biol Biochem 43:1812–1836

Lei C, Sun Y, Khan E, Chen SS, Tsang DC, Graham NJ, Ok YS, Yang X, Lin D, Feng Y (2018) Removal of chlorinated organic solvents from hydraulic fracturing wastewater by bare and entrapped nanoscale zero-valent iron. Chemosphere 196:9–17

Lian F, Sun B, Song Z, Zhu L, Qi X, Xing B (2014) Physicochemical properties of herb-residue biochar and its sorption to ionizable antibiotic sulfamethoxazole. Chem Eng J 248:128–134

Lian F, Sun B, Chen X, Zhu L, Liu Z, Xing B (2015) Effect of humic acid (HA) on sulfonamide sorption by biochars. Environ Pollut 204:306–312

Liao P, Zhan Z, Dai J, Wu X, Zhang W, Wang K, Yuan S (2013) Adsorption of tetracycline and chloramphenicol in aqueous solutions by bamboo charcoal: a batch and fixed-bed column study. Chem Eng J 228:496–505

Lin Y, Xu S, Li J (2013) Fast and highly efficient tetracyclines removal from environmental waters by graphene oxide functionalized magnetic particles. Chem Eng J 225:679–685

Liu P, Liu W-J, Jiang H, Chen J-J, Li W-W, Yu H-Q (2012) Modification of bio-char derived from fast pyrolysis of biomass and its application in removal of tetracycline from aqueous solution. Biores Technol 121:235–240

Liu X, Zhou Y, Zhang J, Luo L, Yang Y, Huang H, Peng H, Tang L, Mu Y (2018) Insight into electro-Fenton and photo-Fenton for the degradation of antibiotics: mechanism study and research gaps. Chem Eng J 347:379–397

Long X-Y, Li J-Y, Sheng D, Lian H-Z (2017) Spinel-type manganese ferrite ($MnFe_2O_4$) microspheres: A novel affinity probe for selective and fast enrichment of phosphopeptides. Talanta 166:36–45

Oleszczuk P, Xing B (2011) Influence of anionic, cationic and nonionic surfactants on adsorption and desorption of oxytetracycline by ultrasonically treated and non-treated multiwalled carbon nanotubes. Chemosphere 85:1312–1317

Parolo ME, Savini MC, Valles JM, Baschini MT, Avena MJ (2008) Tetracycline adsorption on montmorillonite: pH and ionic strength effects. Appl Clay Sci 40:179–186

Peng X, Hu F, Zhang T, Qiu F, Dai H (2018) Amine-functionalized magnetic bamboo-based activated carbon adsorptive removal of ciprofloxacin and norfloxacin: a batch and fixed-bed column study. Biores Technol 249:924–934

Pezoti O, Cazetta AL, Bedin KC, Souza LS, Martins AC, Silva TL, Júnior OOS, Visentainer JV, Almeida VC (2016) NaOH-activated carbon of high surface area produced from guava seeds as a high-efficiency adsorbent for amoxicillin removal: kinetic, isotherm and thermodynamic studies. Chem Eng J 288:778–788

Reddy DHK, Yun Y-S (2016) Spinel ferrite magnetic adsorbents: alternative future materials for water purification? Coord Chem Rev 315:90–111

Shakoor MB, Niazi NK, Bibi I, Shahid M, Saqib ZA, Nawaz MF, Shaheen SM, Wang H, Tsang DCW, Bundschuh J, Ok YS, Rinklebe J (2019) Exploring the arsenic removal potential of various biosorbents from water. Environ Int 123:567–579

Shen Z, Zhang J, Hou D, Tsang D, Ok YS, Alessi D (2018) Synthesis of MgO-coated corncob biochar and its application in lead stabilization in a soil washing residue. Environ Int 122:357–362

Silber A, Levkovitch I, Graber E (2010) pH-dependent mineral release and surface properties of cornstraw biochar: agronomic implications. Environ Sci Technol 44:9318–9323

Sillanpää ME, Kurniawan TA, Lo W-h (2011) Degradation of chelating agents in aqueous solution using advanced oxidation process (AOP). Chemosphere 83:1443–1460

Singh R, Bishnoi NR, Kirrolia A (2013) Evaluation of Pseudomonas aeruginosa an innovative bioremediation tool in multi metals ions from simulated system using multi response methodology. Biores Technol 138:222–234

Spokas KA, Reicosky DC (2009) Impacts of sixteen different biochars on soil greenhouse gas production. Ann Environ Sci 3:179–193

Sun Y, Cho D-W, Graham NJ, Hou D, Yip AC, Khan E, Song H, Li Y, Tsang DC (2019a) Degradation of antibiotics by modified vacuum-UV based processes: mechanistic consequences of H_2O_2 and $K_2S_2O_8$ in the presence of halide ions. Sci Total Environ 664:312–321

Sun Y, Iris K, Tsang DC, Cao X, Lin D, Wang L, Graham NJ, Alessi DS, Komárek M, Ok YS (2019b) Multifunctional iron-biochar composites for the removal of potentially toxic elements, inherent cations, and hetero-chloride from hydraulic fracturing wastewater. Environ Int 124:521–532

Taheran M, Naghdi M, Brar SK, Knystautas EJ, Verma M, Ramirez AA, Surampalli RY, Valéro JR (2016) Adsorption study of environmentally relevant concentrations of chlortetracycline on pinewood biochar. Sci Total Environ 571:772–777

Tan X-f, Liu Y-g, Gu Y-l, Xu Y, Zeng G-m, Hu X-j, Liu S-b, Wang X, Liu S-m, Li J (2016) Biochar-based nano-composites for the decontamination of wastewater: a review. Biores Technol 212:318–333

Tang L, Feng H, Tang J, Zeng G, Deng Y, Wang J, Liu Y, Zhou Y (2017) Treatment of arsenic in acid wastewater and river sediment by Fe@ Fe_2O_3 nanobunches: the effect of environmental conditions and reaction mechanism. Water Res 117:175–186

Tang L, Yu J, Pang Y, Zeng G, Deng Y, Wang J, Ren X, Ye S, Peng B, Feng H (2018) Sustainable efficient adsorbent: alkali-acid modified magnetic biochar derived from sewage sludge for aqueous organic contaminant removal. Chem Eng J 336:160–169

Tian C, Zhao J, Zhang J, Chu S, Dang Z, Lin Z, Xing B (2017) Enhanced removal of roxarsone by Fe_3O_4@3D graphene nanocomposites: synergistic adsorption and mechanism. Environ Sci Nano 4:2134–2143

Wang H, Yao Q, Wang C, Ma Z, Sun Q, Fan B, Jin C, Chen Y (2017) Hydrothermal synthesis of nanooctahedra $MnFe_2O_4$ onto the wood surface with soft magnetism, fire resistance and electromagnetic wave absorption. Nanomaterials 7:118

Wen B, Li R-j, Zhang S, Shan X-q, Fang J, Xiao K, Khan SU (2009) Immobilization of pentachlorophenol in soil using carbonaceous material amendments. Environ Pollut 157:968–974

Xiang Y, Xu Z, Wei Y, Zhou Y, Yang X, Yang Y, Yang J, Zhang J, Luo L, Zhou Z (2019a) Carbon-based materials as adsorbent for antibiotics removal: mechanisms and influencing factors. J Environ Manage 237:128–138

Xiang Y, Xu Z, Zhou Y, Wei Y, Long X, He Y, Zhi D, Yang J, Luo L (2019) A sustainable ferromanganese biochar adsorbent for effective levofloxacin removal from aqueous medium. Chemosphere 237:124464

Xiang Y, Yang X, Xu Z, Hu W, Zhou Y, Wan Z, Yang Y, Wei Y, Yang J, Tsang DC (2020) Fabrication of sustainable manganese ferrite modified biochar from vinasse for enhanced adsorption of fluoroquinolone antibiotics: effects and mechanisms. Sci Total Environ 709:136079

Xiang Y, Jiang L, Zhou Y, Luo Z, Zhi D, Yang J, Lam SS (2022) Microplastics and environmental pollutants: key interaction and toxicology in aquatic and soil environments. J Hazard Mater 422:126843

Xiao Y, Liang H, Chen W, Wang Z (2013) Synthesis and adsorption behavior of chitosan-coated $MnFe_2O_4$ nanoparticles for trace heavy metal ions removal. Appl Surf Sci 285:498–504

Xiao Y, Tsibart A, Nam H, Hur J, El-Naggar A, Tack F, Wang C-H, Lee Y, Tsang D, Ok YS (2019) Effect of gasification biochar application on soil quality: trace metal behavior, microbial community, and soil dissolved organic matter. J Hazard Mater 365:684–669

Xie M, Shon HK, Gray SR, Elimelech M (2016) Membrane-based processes for wastewater nutrient recovery: technology, challenges, and future direction. Water Res 89:210–221

Xiong W, Zeng G, Yang Z, Zhou Y, Zhang C, Cheng M, Liu Y, Hu L, Wan J, Zhou C (2018) Adsorption of tetracycline antibiotics from aqueous solutions on nanocomposite multi-walled carbon nanotube functionalized MIL-53 (Fe) as new adsorbent. Sci Total Environ 627:235–244

Xu Z, Xiang Y, Zhou H, Yang J, He Y, Zhu Z, Zhou Y (2021) Manganese ferrite modified biochar from vinasse for enhanced adsorption of levofloxacin: effects and mechanisms. Environ Pollut 272:115968

Yang F, Zhang S, Sun Y, Tsang DC, Cheng K, Ok YS (2019) Assembling biochar with various layered double hydroxides for enhancement of phosphorus recovery. J Hazard Mater 365:665–673

Yao H, Lu J, Wu J, Lu Z, Wilson PC, Shen Y (2013a) Adsorption of fluoroquinolone antibiotics by wastewater sludge biochar: role of the sludge source. Water Air Soil Pollut 224:1370

Yao Y, Gao B, Chen J, Yang L (2013b) Engineered biochar reclaiming phosphate from aqueous solutions: mechanisms and potential application as a slow-release fertilizer. Environ Sci Technol 47:8700–8708

Yu F, Li Y, Han S, Ma J (2016) Adsorptive removal of antibiotics from aqueous solution using carbon materials. Chemosphere 153:365–385

Zhang Q-Q, Ying G-G, Pan C-G, Liu Y-S, Zhao J-L (2015) Comprehensive evaluation of antibiotics emission and fate in the river basins of China: source analysis, multimedia modeling, and linkage to bacterial resistance. Environ Sci Technol 49:6772–6782

Zhang Z, Wang Y, Tan Q, Zhong Z, Su F (2013) Facile solvothermal synthesis of mesoporous manganese ferrite (MnFe$_2$O$_4$) microspheres as anode materials for lithium-ion batteries. J Colloid Interface Sci 398:185–192

Zhao Y, Gu X, Gao S, Geng J, Wang X (2012) Adsorption of tetracycline (TC) onto montmorillonite: cations and humic acid effects. Geoderma 183:12–18

Zhou Y, Liu X, Xiang Y, Wang P, Zhang J, Zhang F, Wei J, Luo L, Lei M, Tang L (2017) Modification of biochar derived from sawdust and its application in removal of tetracycline and copper from aqueous solution: adsorption mechanism and modelling. Biores Technol 245:266–273

Zhou Y, Xiang Y, He Y, Yang Y, Zhang J, Luo L, Peng H, Dai C, Zhu F, Tang L (2018) Applications and factors influencing of the persulfate-based advanced oxidation processes for the remediation of groundwater and soil contaminated with organic compounds. J Hazard Mater 359:396–407

Zhou Y, He Y, He Y, Liu X, Xu B, Yu J, Dai C, Huang A, Pang Y, Luo L (2019a) Analyses of tetracycline adsorption on alkali-acid modified magnetic biochar: site energy distribution consideration. Sci Total Environ 650:2260–2266

Zhou Y, He Y, Xiang Y, Meng S, Liu X, Yu J, Yang J, Zhang J, Qin P, Luo L (2019b) Single and simultaneous adsorption of pefloxacin and Cu (II) ions from aqueous solutions by oxidized multiwalled carbon nanotube. Sci Total Environ 646:29–36

Publisher's note Springer Nature remains neutral with regard to jurisdictional claims in published maps and institutional affiliations.